A Reduced Set of Air Plasma Reactions for Nanosecond Pulsed Plasmas

Moon Soo Bak and Mark A. Cappelli

***Abstract*— The reduction of a mechanism describing plasma chemistry for dry air has been carried out for conditions of nanosecond-pulsed discharge plasmas. The discharge conditions include both diffuse glow and filamentary spark modes. A reduced set for glow discharges is found to have inelastic electron-impact reactions of N_2 and O_2, quenching of excited N_2, electron attachment to O_2^-, ion conversion between N_2^+, N_4^+, O_4^+, $O_2^+ \cdot N_2$, and O_2^+, and ion–ion and electron–ion recombination. When the discharge is in a filamentary mode, additional reactions are required beyond those for the glow discharge as a result of the increased electron number density and high levels of molecular dissociation. Those additional reactions include electron-impact excitation of N and O, quenching of excited N_2 by N and O, and associative ionization by collisions between excited N_2. A significant reduction in the number of species and reactions is obtained without compromising the predicted species' number densities and temperature. These results provide researchers with reduced kinetic mechanisms that high-fidelity simulations could rely on to save computational time.**

***Index Terms*— Plasma chemistry, plasma simulation.**

I. Introduction

HIGHLY nonequilibrium nanosecond pulsed discharges that have been generated at relatively high pressures have been shown to have a lower power budget than other methods in forming plasmas of high electron densities [1]. For over a decade now, these types of nonequilibrium discharges have been used to enhance and stabilize combustion [2]–[5] and to actuate aerodynamic flows [6]–[9]. These applications take advantage of the high reactivity of the plasma to promote new chemical pathways, or the highly ionized state as a means to transfer momentum to the background air flow. High-fidelity numerical simulations of plasma-assisted combustion or plasma actuation of air flows require a detailed understanding of the plasma kinetics. Equally important is the need to develop reduced yet accurate kinetic mechanisms so as to reduce the computational time. In this paper, we describe a reduced kinetic mechanism that captures all of the critical kinetic pathways seen in the use of much larger mechanisms that have been described in [10].

Manuscript received December 22, 2014; revised February 10, 2015; accepted February 27, 2015. Date of publication March 16, 2015; date of current version April 13, 2015. This work was supported in part by the National Science Foundation (NSF) and in part by the Department of Energy (DOE) through the NSF/DOE Partnership in Basic Plasma Science.

M. S. Bak was with Stanford University, Stanford, CA 94305 USA. He is now with the School of Mechanical Engineering, Sungkyunkwan University, Suwon 440-746, Korea (e-mail: moonsoo@skku.edu).

M. A. Cappelli is with the Department of Mechanical Engineering, Stanford University, Stanford, CA 94305 USA (e-mail: cap@stanford.edu).

Color versions of one or more of the figures in this paper are available online at http://ieeexplore.ieee.org.

Digital Object Identifier 10.1109/TPS.2015.2409300

While several mechanisms have been proposed that describe plasma air chemistry [11]–[15], some of which have been tested against the experimental data [11]–[13], one that is commonly encountered in the literature is [10], which is specifically developed for plasma discharges in dry air. Despite the limited validation of this mechanism, the reactions included in its kinetic subsets were not systematically chosen and the mechanisms have not been tested for a broad range of conditions.

Many studies have been carried out on the reduction in the number of species and reactions that are needed to describe hydrocarbon combustion chemistry [16], [17]. In general, the complexity of a reaction mechanism increases exponentially as the number of species increases. A systematic reduction in the size of the mechanism can save considerable computational expense. Despite the several reduced mechanisms available for combustion [16], [17], a very few studies have been carried out for reducing plasma reaction mechanisms [18], [19]. In this paper, we report on the performance of a reduced kinetic mechanism that is used to describe air plasma chemistry, in particular, that driven by a nonequilibrium nanosecond pulsed discharge [20]–[22]. Our approach that is used is a method that is sometimes referred to as detailed reduction in the combustion chemistry literature [16]. The method is tested under conditions comparable with what is found in nanosecond pulsed discharges operating in either a diffuse glow mode [20] or in a filamentary spark mode [21]. We show that in the later regime, the increased plasma density requires including additional reactions that are not necessary for conditions of lower plasma density. Since nanosecond pulsed plasmas are now used for combustion and flow control at high pressures (>1 atm) [5], [8], [9], it is important to understand the reaction pathways relevant to relatively high plasma densities, particularly when $n_e \gg 10^{14}$ cm^{-3}.

II. Computation Detail

The method of detailed reduction [16] is applied here to the mechanism proposed in [10] that describes plasma reactions in dry air. Detailed reduction requires calculating all of the elementary reaction rates and associated heating rates for forward and reverse reactions that are in the detailed (starting) mechanism. These rates are then compared against the maximum rates at the given time to sort out important reactions. Since a reaction rate is a strong function of gas temperature and electric field, the importance of each reaction varies during the reaction time. Reactions that will ultimately be included in a reduced mechanism are, therefore, selected

when each reaction satisfies the criteria of

$$|R_i| > \varepsilon_R |R_{\max}| \tag{1}$$

$$|R_i H_i| > \varepsilon_Q |Q_{\max}| \tag{2}$$

at any of the tested times. The parameters, ε_R and ε_Q, determine the ultimate number of reactions and species in the reduced mechanism, and their values are typically set to be significantly smaller than unity. In this paper, we set $\varepsilon_R = \varepsilon_Q = 10^{-2}$. In (1) and (2), R_i is the rate of reaction i, $R_{\max}$ is the maximum reaction rate, H_i is the heating rate of reaction i, and $Q_{\max}$ is the maximum heating rate. It is noteworthy that in applying the criteria we categorize reactions into two subsets (one that contains ionized particles in the reaction and the other that does not). This is because the former reactions tend to have smaller rates although those reactions determine the electron population and plasma behavior.

The detailed reaction mechanism in [10] consists of 46 species and 445 reactions. When counting species, we consider each excited (electronic or ionized) state as different species. The species in the mechanism are electron (e), N_2 (X, A, B, a′, C), O_2 (X, a, b, c, C, A), N, N (^{2}D, ^{2}P), O, O (^{1}D, ^{1}S), O_3, NO, NO_2, NO_3, N_2O, N_2O_4, N_2O_5, N_2^+, O_2^+, N^+, O^+, NO^+, N_3^+, N_4^+, O_4^+, $O_2^+ \cdot N_2$, $NO^+ \cdot N_2$, $NO^+ \cdot O_2$, $NO^+ \cdot NO$, NO_2^+, N_2O^+, O_2^-, O^-, O_3^-, O_4^-, NO^-, NO_2^-, NO_3^-, NO_3^{*-}, and N_2O^-. The reactions are classified into: 1) inelastic electron-impact processes (i.e., electronic excitation, dissociation, and ionization); 2) associative ionization; 3) recombination between electrons and positive ions; 4) electron attachment and detachment; 5) quenching of electronically excited species; 6) ion conversion; 7) recombination between positive and negative ions; and 8) other reactions between neutral species in their ground state. The complete description of reactions is provided in [10]. Most of the reaction rate coefficients, except those for electron-impact reactions, are adapted from [10]. Those for the electron-impact reactions are tabulated as a function of the reduced electric field (E/n). We use cross-sectional data for the electron impact of N_2 [23], O_2 [24], N [25], and O [26]. The computation of the electron energy distribution function and the reaction rate coefficients is facilitated using the Boltzmann equation solver, *BOLSIG* + [27].

As mentioned above, two different plasma conditions are studied here. One is that of a typical diffuse glow discharge and the other is that of a filamentary spark discharge. The glow discharge plasma is in general achieved by either preheating the base flow or lowering the pressure. Similar to [20]–[22], our modeled voltage pulse has a trapezoidal shape in time with a 3-ns rise time, a 4-ns fall time, and a 10-ns plateau, as shown in Fig. 1. The peak voltage, electrode spacing, and gas temperature are chosen to be 6.7 kV, 5 mm, and 1100 K for the glow discharge and 7.3 kV, 5 mm, and 1000 K for the filamentary discharge. The base flow (e.g., co-flow) refreshes the discharge region and its speed is taken to be 2 m/s.

The simulation that is carried out here to test the kinetic mechanism is quasi-0-D. The schematic of the simulation is shown in Fig. 1 (top). The plasma reactions progress while species from the surrounding flow enter and exit the finite

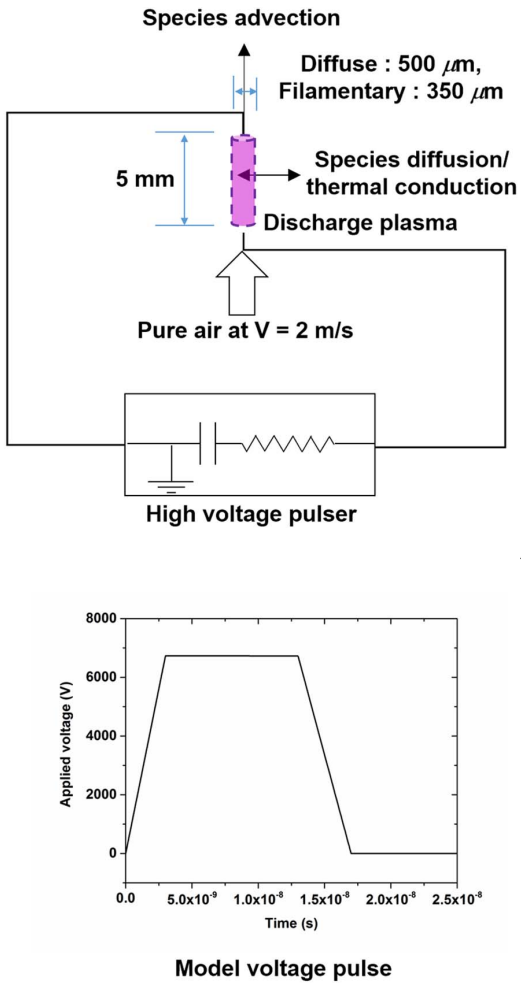

Fig. 1. Schematic of the discharge simulation (top) and the model voltage pulse applied between electrodes separated by 5 mm (bottom). The corresponding peak voltage is used to form a glow discharge.

discharge region through diffusion and advection processes. We assume that the discharge is spatially uniform although it is true that the electric field in the near cathode region is stronger than that in the bulk region of the plasma. A pulsing circuit is also considered in the simulation since in a filamentary mode, the electrical current associated with the plasma can be sufficiently high so as to affect the voltage drop across the electrodes.

In the computations, the species conservation equations

$$\frac{dn_j}{dt} = \sum_{\text{reactions}} (\nu_j' - \nu_j) \left[k_f \prod_i n_{\text{reac},i}^{\nu_i} - k_b \prod_i n_{\text{prod},i}^{\nu_i'} \right] - D_j \frac{n_{\text{total}} + n_{\text{total,coflow}}}{2} \frac{c_j - c_{j,\text{coflow}}}{R^2} - V_c \frac{n_j^*}{R/2} + V_{\text{adv}} \frac{n_{j,\text{initial}}}{L} - V_{\text{adv}}^* \frac{n_j}{L} \tag{3}$$

for a reaction

$$\sum_i \nu_i n_{\text{reac},i} \underset{k_b}{\overset{k_f}{\rightleftharpoons}} \sum_i \nu_i' n_{\text{prod},i} \tag{4}$$

are solved together with an overall energy equation (5), as shown at the bottom of the next page.

In (3)–(5), n_j and c_j are the number density and mole fraction of species j, n_{total} is the total number density, ν_j, $c_{v,j}$, and $h_{f,j}$ and $h_{s,j}$ are the corresponding stoichiometric coefficients, heat capacity (at constant volume), and formation and sensible enthalpies. We note that we take $h^{\dagger}_{s,j} = h_{s,j}$ if $c_j - c_{j,\text{coflow}} > 0$, otherwise $h^{\dagger}_{s,j} = h_{s,j,\text{coflow}}$, and $n^*_j = n_j$ and $h^*_{s,j} = h_{s,j}$ if $V_c > 0$, otherwise $n^*_j = n_{j,\text{coflow}}$ and $h^*_{s,j} = h_{s,j,\text{coflow}}$. In addition, in these equations, k_f and k_b are the forward and reverse reaction rate coefficients, T is the gas temperature, E is the electric field, e is the electron charge, μ_e is the electron mobility, D_j is the diffusion coefficient of species j, k is the thermal conductivity, V_{adv} is the initial advection velocity, and R and L are the effective lengths for diffusion and advection, respectively. V_c and V^*_{adv} are the local convection and advection velocities, calculated to satisfy

$$V_c = \frac{\sum_{\text{species},j} -D_j M_j \frac{n_{\text{total}}+n_{\text{total,coflow}}}{2} \frac{c_j - c_{j,\text{coflow}}}{2R}}{\sum_{\text{species},j} M_j n^*_j} \tag{6}$$

and

$$V^*_{\text{adv}} = \frac{\rho_{\text{initial}}}{\rho} V_{\text{adv}}. \tag{7}$$

Here, M_j is the molecular weight of species j and ρ is the gas density. In (5), the first term of right-hand side accounts for joule heating of the electrons within the discharge, and the second and third terms of the right-hand side describe the volumetric rate of net energy gain as a result of reactions and species diffusion/advection and thermal conduction to the surrounding flow.

As mentioned earlier, the pulsing circuit is included in the simulation. The circuit is modeled as a discharging capacitor across a resistive load, and the consequential effect of a voltage drop across the load as the current charges the high-voltage capacitor is accounted for when calculating the reduced electric field. The energy stored in the capacitor bank (W) is assumed to be 1 mJ. The effective capacitance (C_{pulser}) of the pulser corresponding to the programmed voltage (V_p) is, therefore, expressed as

$$C_{\text{pulser}}(t) = \frac{2W}{V_p(t)^2}. \tag{8}$$

The actual voltage after reflecting the charge accumulation into the capacitor is calculated by

$$V = V_p - \frac{Q_e}{C_{\text{pulser}}} - en_e\mu_e E A_d Z \tag{9}$$

TABLE I
REACTIONS OF A REDUCED SET TO SIMULATE THE KINETICS OF DIFFUSE GLOW DISCHARGES IN DRY AIR

	Reaction	Reference
R1*	N_2+e→N_2(A)+e	[23]
R2*	N_2+e→N_2(B)+e	[23]
R3*	N_2+e→N_2(a')+e	[23]
R4*	N_2+e→N_2(C)+e	[23]
R5*	O_2+e→2O+e	[24]
R6*	O_2+e→O+O(^{1}D)+e	[24]
R7*	N_2+e→N_2^++2e	[23]
R8*	O_2+e→O_2^++2e	[24]
R9*	O_2+e→O^-+O	[24]
R10*	O_2^++e→2O	[10]
R11	e+2O_2→O_2^-+O_2	[10]
R12	O_2^-+O→O_3+e	[10]
R13*	O^-+O→O_2+e	[10]
R14	O_3^-+O→2O_2+e	[10]
R15	O_2^-+N_2→O_2+N_2+e	[10]
R16	O_2^-+O_2→2O_2+e	[10]
R17	O+O_3→2O_2	[10]
R18	O+O_2+M→O_3+M	[10]
R19*	N_2(A)+O_2→N_2+2O	[10]
R20	N_2(A)+O_2→N_2O+O	[10]
R21*	N_2(A)+O_2→N_2+O_2	[10]
R22*	N_2(B)+N_2→N_2(A)+N_2	[10]
R23*	N_2(B)+O_2→N_2+2O	[10]
R24*	N_2(a')+N_2→N_2(B)+N_2	[10]
R25*	N_2(a')+O_2→N_2+2O	[10]
R26*	N_2(C)→N_2(B)+hν	[10]
R27*	N_2(C)+N_2→N_2(a')+N_2	[10]
R28*	N_2(C)+O_2→N_2+2O	[10]
R29*	O(^{1}D)+N_2→O+N_2	[10]
R30*	O(^{1}D)+O_2→O+O_2	[10]
R31*	N_2^++2N_2→N_4^++N_2	[10]
R32	O_2^++2N_2→O_2^+·N_2+N_2	[10]
R33	O_2^++2O_2→O_4^++O2	[10]
R34*	N_4^++O_2→O_2^++2N_2	[10]
R35	O_4^++N_2→O_2^+·N_2+O_2	[10]
R36	O_4^++O_2→O_2^++2O_2	[10]
R37	O_2^+·N_2+N_2→O_2^++2N_2	[10]
R38	O_2^+·N_2+O_2→O_4^++N_2	[10]
R39	O_2^-+O_2+M→O_4^-+M	[10]
R40	O_2^-+O→O_2+O^-	[10]
R41	O_3^-+O→O_2^-+O_2	[10]
R42	O^-+O_2+M→O_3^-+M	[10]
R43	O_4^-+M→O_2^-+O_2+M	[10]
R44	O_2^-+O_2^+→2O_2	[10]
R45	O^-+O_2^+→O+O_2	[10]
R46	O_3^-+O_2^+→O_3+O_2	[10]
R47	O_2^-+O_2^+→O_2+2O	[10]
R48	O_3^-+O_2^+→O_3+2O	[10]
R49	O_2^-+O_2^++M→2O_2+M	[10]

and

$$Q_e(t) = \int_0^t en_e\mu_e E A_d dt'. \tag{10}$$

The output impedance of the pulser (Z) is assumed to be 100 Ω. Since the simulation is quasi-0-D and computes the

$$\sum_{\text{species}j} \frac{d\left(c_{v,j} n_j T\right)}{dt} = en_e\mu_e E^2 + \sum_{\text{species}j} \begin{bmatrix} -h_{f,j}\frac{dn_j}{dt} \\ -D_j h^{\dagger}_{s,j} \frac{n_{\text{total}}+n_{\text{total,coflow}}}{2} \frac{c_j - c_{j,\text{coflow}}}{R^2} \\ -V_c \frac{h^*_{s,j} n^*_j}{R/2} \\ +V_{\text{adv}} \frac{h_{s,j,\text{initial}} n_{j,\text{initial}}}{L} - V^*_{\text{adv}} \frac{h_{s,j} n_j}{L} \end{bmatrix} - k\frac{T - T_{\text{coflow}}}{R^2} \tag{5}$$

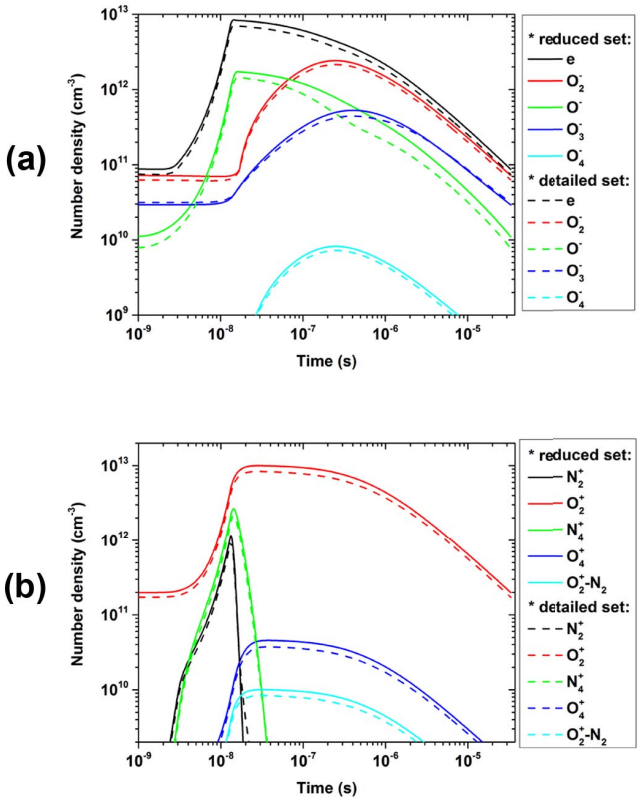

Fig. 2. Comparison for the time histories of (a) negatively charged species and (b) positively charged species densities calculated using a full reaction set and the reduced set when the discharge is in diffuse glow mode.

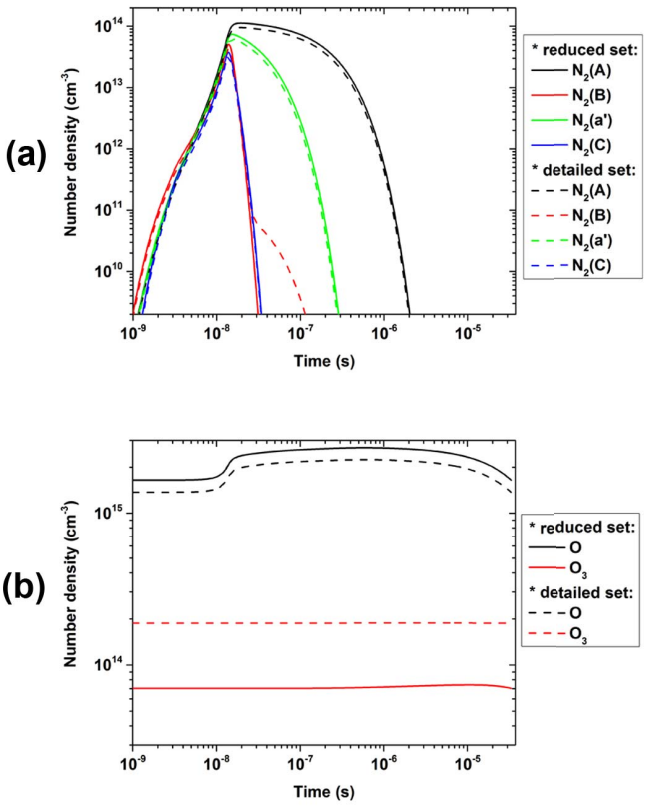

Fig. 3. Comparison for the time histories of (a) N_2 (A, B, a′, C) and (b) O and O_3 densities calculated using a full reaction set and the reduced set when the discharge is in diffuse glow mode.

current density, the cross-sectional area of the discharge (A_d) is required to estimate the current. From the previous experimental results, the diameters of 500 and 350 μm are used for the glow and filamentary discharges [22].

The mechanism reduction is carried out at various times within the discharge pulse to validate it over the entire period. The selected times are 1.5 ns, 8 ns, 15 ns, 200 ns, 2 μs, and 20 μs. As explained before, the final reduced mechanism includes all of the reactions that satisfy the criteria for all of these times. As we simulate the repetitive discharges, the simulation is carried out for a series of pulses rather than a single pulse. This is because excluding some potentially important plasma reactions could result in a different quasi-steady state for species densities and temperature. The results shown in this paper are for a train of 50 pulses, during which initial number densities of species and gas temperature reach their quasi-steady-state values.

III. Results

The mechanism reduction is first carried out for the low plasma density (glow discharge) case. The reduced mechanism is determined to require 20 species of e, N_2 (X, A, B, a′, C), O_2, O, O(^{1}D), O_3, N_2O, N_2^+, O_2^+, N_4^+, O_4^+, $O_2^+ \cdot N_2$, O_2^-, O^-, O_3^-, and O_4^- and 49 reactions listed in Table I. We note that excited states of O_2 and their reactions are not included in the reduced set since their contribution to chain-breaking reactions and temperature is small. From Table I, most of the electron-impact inelastic collisions of N_2 and O_2 (i.e., electronic excitation, dissociation, and ionization) are found to be important. As a result, quenching of the excited states of N_2 (A, B, a′, C) is also important. It is notable that there is a significant reduction in the number of reactions needed to describe ion conversion and electron–ion recombination. Dominant ion conversion pathways are found to be $R31$–$R38$ through which N_2^+ transfers its charge to N_4^+, O_4^+, and $O_2^+ \cdot N_2$, and finally to form O_2^+. The O_2^+ then recombines with electrons ($R10$) and negative ions of O_2^-, O^-, and O_3^- ($R44$–$R49$). This reduced set is somewhat similar to that proposed in [19] that is obtained from a sensitivity analysis of the importance of individual reactions to gas heating.

Time histories of species' number densities calculated by the simulation with the reduced reaction mechanism are compared with those calculated with the detailed mechanism to provide a sense of how accurately the reduced mechanism reproduces the results of the detailed mechanism. Comparisons for negatively charged species (e, O_2^-, O^-, O_3^-, and O_4^-) and positively charged species (N_2^+, O_2^+, N_4^+, O_4^+, and $O_2^+ \cdot N_2$) densities are shown in Fig. 2(a) and (b), respectively. Comparisons for N_2 (A, B, a′, C) and O and O_3 are shown in Fig. 3(a) and (b), respectively. The calculation carried out with the reduced set is found to reach a quasi-steady state over tens of pulses and also appears to be in good agreement with the species time traces that are obtained from the detailed mechanism. For all of the species except O_3, the reduced set slightly overestimates the number density. This is attributed to a slightly elevated

TABLE II
REACTIONS REQUIRED IN ADDITION TO THOSE IN TABLE I TO SIMULATE THE KINETICS OF FILAMENTARY SPARK DISCHARGES IN DRY AIR

	Reaction	Reference
R50	$N+e \rightarrow N(^2D)+e$	[25]
R51	$O+e \rightarrow O(^1D)+e$	[26]
R52	$O+e \rightarrow O(^1S)+e$	[26]
R53	$N_2^+ + e \rightarrow N+N$	[10]
R54	$N_2^+ + e \rightarrow N+N(^2D)$	[10]
R55	$N_4^+ + e \rightarrow 2N_2$	[10]
R56	$NO^+ + e \rightarrow N(^2D)+O$	[10]
R57	$N_2(A)+N_2(a') \rightarrow N_4^+ + e$	[10]
R58	$N_2(a')+N_2(a') \rightarrow N_4^+ + e$	[10]
R59	$N+O_2 \rightarrow NO+O$	[10]
R60	$N+NO \rightarrow N_2+O$	[10]
R61	$N_2(A)+O \rightarrow NO+N(^2D)$	[10]
R62	$N_2(A)+O \rightarrow N_2+O(^1S)$	[10]
R63	$N_2(A)+N \rightarrow N_2+N(^2P)$	[10]
R64	$N_2(A)+NO \rightarrow N_2+NO$	[10]
R65	$N_2(a')+NO \rightarrow N_2+N+O$	[10]
R66	$N(^2D)+O_2 \rightarrow NO+O$	[10]
R67	$N(^2D)+O_2 \rightarrow NO+O(^1D)$	[10]
R68	$N(^2P)+O_2 \rightarrow NO+O$	[10]
R69	$O(^1D)+NO \rightarrow N+O_2$	[10]
R70	$O(^1S)+O \rightarrow O(^1D)+O$	[10]
R71	$N_4^+ + N_2 \rightarrow N_2^+ + 2N_2$	[10][a]
R72	$O_2^+ + N \rightarrow NO^+ + O$	[10]
R73	$O_2^+ + NO \rightarrow NO^+ + O_2$	[10]

[a] This rate coefficient is assumed not to exceed 2.5×10^{10} cm^{-3}.

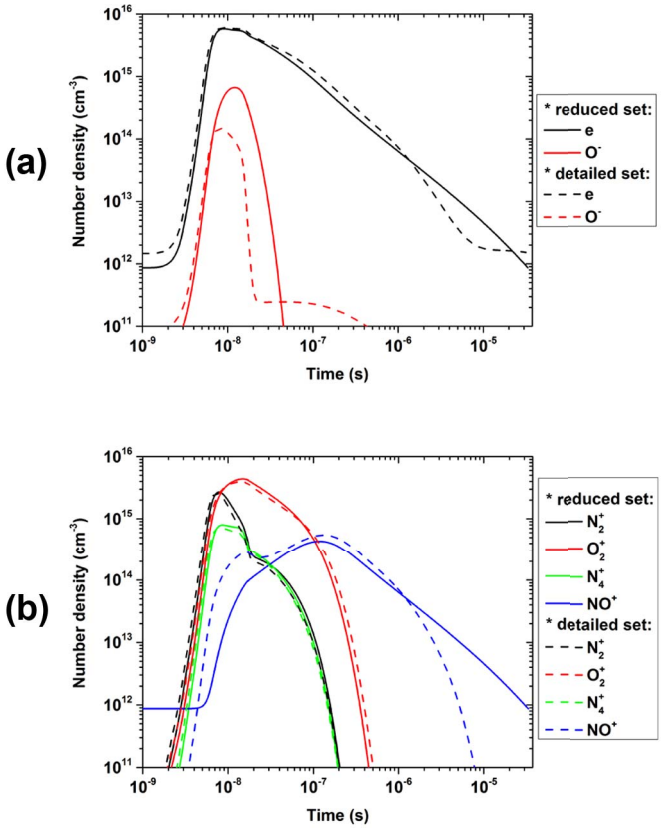

Fig. 4. Comparison for the time histories of (a) negatively charged species and (b) positively charged species densities calculated using a full reaction set and its reduced set when the discharge is in filamentary mode.

electron number density that is maintained between pulses. For this glow mode simulation, the electron density peaks at about 9×10^{12} cm^{-3}, and the temperature increase beyond

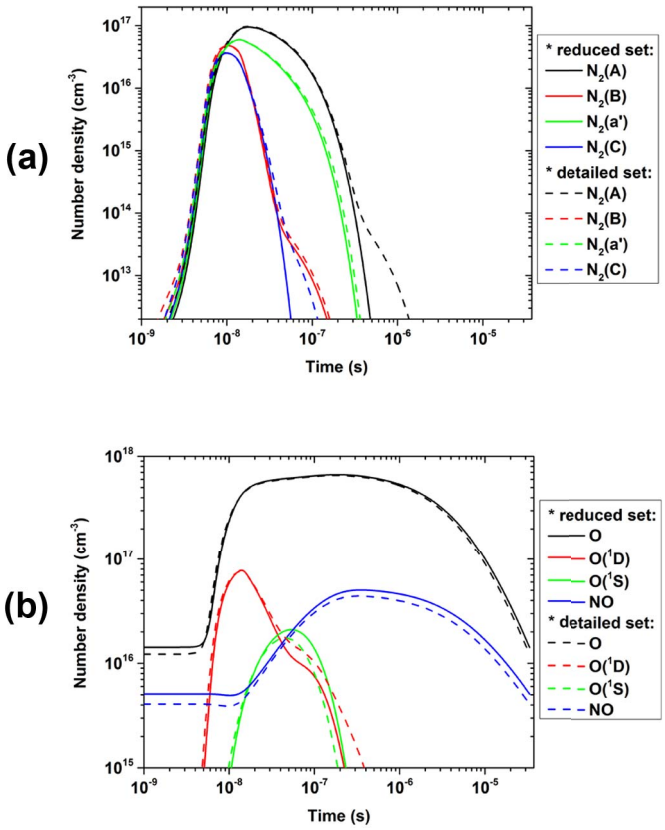

Fig. 5. Comparison for the time histories of (a) N_2 (A, B, a′, C) and (b) O, O (^{1}D), O(^{1}S), and NO densities calculated using a full reaction set and its reduced set when the discharge is in filamentary mode.

the initial 1100 K was found to be negligible (e.g., about 4 K, not shown).

The mechanism reduction is then carried out for the high plasma density (filamentary discharge mode) case. The reduced mechanism under these conditions requires 19 species [e, N_2 (X, A, B, a′, C), O_2, N, N(^{2}D, ^{2}P), O, O(^{1}D, ^{1}S), NO, N_2^+, O_2^+, N_4^+, NO^+, and O^-] and the reactions listed in Table II, in addition to those with asterisk in Table I (total of 48 reactions). Compared with the low plasma density case, we find that the high plasma density case requires the contributions of dissociated species and the quenching of excited species by these dissociated species to the chemistry to obtain good agreement with the results based on the full (detailed) mechanism. The additional required species and reactions are due to the increased level of electron density. For ionization, the contribution of associative ionization (*R*57 and *R*58) to the overall ionization is no longer negligible as the collisions between the excited states of N_2 become likely. Ion conversion pathways are found to be simpler for this type of discharge: N_2^+ transfers its charge to N_4^+ and O_2^+, and finally to NO^+. N_2^+, N_4^+, O_2^+, and NO^+ then recombines with electrons mostly through dissociative recombination. It is noteworthy that NO formation reactions are included into the reduced set since the level of N and O densities is high.

Time histories of species densities calculated by the plasma simulation with the reduced mechanism are compared with those using the detailed mechanism in Figs. 4 and 5. Comparisons for negatively charged species (e and O^-) and positively

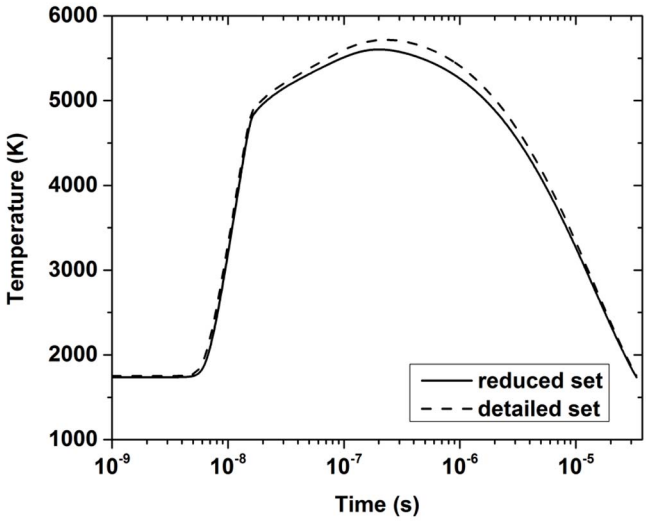

Fig. 6. Comparison for the temperature time histories calculated using a full reaction set and its reduced set when the discharge is in filamentary mode.

charged species (N_2^+, O_2^+, N_4^+, and NO^+) densities are shown in Fig. 4(a) and (b), and comparisons for N_2 (A, B, a′, C) and other products [O, O(^{1}D, ^{1}S), and NO] are shown in Fig. 5(a) and (b), respectively. As seen in the glow discharge case, the proposed reduced set is stable over repetitive pulses and reproduces the results obtained from the full reaction set reasonably well. Slight differences are shown for O^- and NO^+ while they decay below 5×10^{14} cm^{-3}. We see that the electron density peaks at about 6×10^{15} cm^{-3}, and the N_2 (B), N_2 (C), and O number densities reach 6×10^{16}, 3.7×10^{16}, and 6.7×10^{17} cm^{-3}, respectively.

The temperature calculated using the full and reduced reaction sets for the filamentary discharge mode are compared in Fig. 6. As expected, based on the favorable species comparisons, the difference between the temperatures over all times is small. The temperature is found to increase up to 5600 K after the voltage pulse as the excited species relax their internal energy to heat the gas, consistent with [21].

IV. Conclusion

We have demonstrated a reduction in the kinetic mechanism that is often used to describe plasma reactions in dry air. The reduced mechanism was validated for conditions that lead to both diffuse glow and filamentary discharge plasmas driven by high-voltage nanosecond pulses. The reduced mechanism for conditions that lead to the diffuse glow plasma contained electron-impact processes of N_2 and O_2, quenching of excited N_2, electron attachment to O_2^-, ion conversion between N_2^+, O_2^+, N_4^+, O_4^+, and $O_2^+ \cdot N_2$, and ion–ion and electron–ion recombination. For conditions that lead to high density plasma formation, the reduced mechanism was expanded to include electron-impact excitation of N and O, quenching of excited N_2 by N, O, and NO, and associative ionization that results from the collisions between the excited states of N_2. This addition of reactions and relevant species is due to the increased level of electron number density. We expect that our result will provide a reduced yet accurate set that could be employed by high-fidelity simulations. The reduced reaction mechanism also provides insight into the plasma chemistry.

References

[1] C. H. Kruger, C. O. Laux, L. Yu, D. M. Packan, and L. Pierrot, "Nonequilibrium discharges in air and nitrogen plasmas at atmospheric pressure," *Pure Appl. Chem.*, vol. 74, no. 3, pp. 337–347, Mar. 2002.

[2] G. Lou *et al.*, "Ignition of premixed hydrocarbon–air flows by repetitively pulsed, nanosecond pulse duration plasma," *Proc. Combust. Inst.*, vol. 31, no. 2, pp. 3327–3334, Jan. 2007.

[3] N. L. Aleksandrov, S. V. Kindysheva, I. N. Kosarev, S. M. Starikovskaia, and A. Y. Starikovskii, "Mechanism of ignition by non-equilibrium plasma," *Proc. Combust. Inst.*, vol. 32, no. 1, pp. 205–212, 2009.

[4] G. Pilla, D. Galley, D. A. Lacoste, F. Lacas, D. Veynante, and C. O. Laux, "Stabilization of a turbulent premixed flame using a nanosecond repetitively pulsed plasma," *IEEE Trans. Plasma Sci.*, vol. 34, no. 6, pp. 2471–2477, Dec. 2006.

[5] M. S. Bak, H. Do, M. G. Mungal, and M. A. Cappelli, "Plasma-assisted stabilization of laminar premixed methane/air flames around the lean flammability limit," *Combust. Flame*, vol. 159, no. 10, pp. 3128–3137, Oct. 2012.

[6] D. V. Roupassov, A. A. Nikipelov, M. M. Nudnova, and A. Y. Starikovskii, "Flow separation control by plasma actuator with nanosecond pulsed-periodic discharge," *AIAA J.*, vol. 47, no. 1, pp. 168–185, Jan. 2009.

[7] J. Little, K. Takashima, M. Nishihara, I. Adamovich, and M. Samimy, "Separation control with nanosecond-pulse-driven dielectric barrier discharge plasma actuators," *AIAA J.*, vol. 50, no. 2, pp. 350–365, Feb. 2012.

[8] Y. Sung, W. Kim, M. G. Mungal, and M. A. Cappelli, "Aerodynamic modification of flow over bluff objects by plasma actuation," *Experim. Fluids*, vol. 41, no. 3, pp. 479–486, Sep. 2006.

[9] S. Im, H. Do, and M. A. Cappelli, "Dielectric barrier discharge control of a turbulent boundary layer in a supersonic flow," *Appl. Phys. Lett.*, vol. 97, no. 4, pp. 041503-1–041503-3, 2010.

[10] I. A. Kossyi, A. Y. Kostinsky, A. A. Matveyev, and V. P. Silakov, "Kinetic scheme of the non-equilibrium discharge in nitrogen-oxygen mixtures," *Plasma Sour. Sci. Technol.*, vol. 1, no. 3, pp. 207–220, Aug. 1992.

[11] M. Uddi, N. Jiang, I. V. Adamovich, and W. R. Lempert, "Nitric oxide density measurements in air and air/fuel nanosecond pulse discharges by laser induced fluorescence," *J. Phys. D, Appl. Phys.*, vol. 42, no. 7, pp. 075205-1–075205-18, Mar. 2009.

[12] S. Nagaraja, V. Yang, Z. Yin, and I. Adamovich, "Ignition of hydrogen–air mixtures using pulsed nanosecond dielectric barrier plasma discharges in plane-to-plane geometry," *Combust. Flame*, vol. 161, no. 4, pp. 1026–1037, Apr. 2014.

[13] M. S. Bak, W. Kim, and M. A. Cappelli, "On the quenching of excited electronic states of molecular nitrogen in nanosecond pulsed discharges in atmospheric pressure air," *Appl. Phys. Lett.*, vol. 98, no. 1, pp. 011502-1–011502-3, Jan. 2011.

[14] I. V. Adamovich, M. Nishihara, I. Choi, M. Uddi, and W. R. Lempert, "Energy coupling to the plasma in repetitive nanosecond pulse discharges," *Phys. Plasmas*, vol. 16, no. 11, pp. 113505-1–113505-13, 2009.

[15] Y. Zhu, Y. Wu, W. Cui, Y. Li, and M. Jia, "Modelling of plasma aerodynamic actuation driven by nanosecond SDBD discharge," *J. Phys. D, Appl. Phys.*, vol. 46, no. 35, pp. 355205-1–355205-16, Aug. 2013.

[16] H. Wang and M. Frenklach, "Detailed reduction of reaction mechanisms for flame modeling," *Combust. Flame*, vol. 87, nos. 3–4, pp. 365–370, Dec. 1991.

[17] T. Lu and C. K. Law, "A directed relation graph method for mechanism reduction," *Proc. Combust. Inst.*, vol. 30, no. 1, pp. 1333–1341, Jan. 2005.

[18] J. H. Park, E. Pfender, and C. H. Chang, "Reduction of chemical reactions in nitrogen and nitrogen–hydrogen plasma jets flowing into atmospheric air," *Plasma Chem. Plasma Process.*, vol. 20, no. 2, pp. 165–181, Jun. 2000.

[19] J. Poggie, I. Adamovich, N. Bisek, and M. Nishihara, "Numerical simulation of nanosecond-pulse electrical discharges," *Plasma Sour. Sci. Technol.*, vol. 22, no. 1, pp. 015001-1–015001-17, Nov. 2013.

[20] D. Z. Pai, G. D. Stancu, D. A. Lacoste, and C. O. Laux, "Nanosecond repetitively pulsed discharges in air at atmospheric pressure—The glow regime," *Plasma Sour. Sci. Technol.*, vol. 18, no. 4, pp. 045030-1–045030-7, Oct. 2009.

[21] D. Z. Pai, D. A. Lacoste, and C. O. Laux, "Nanosecond repetitively pulsed discharges in air at atmospheric pressure—The spark regime," *Plasma Sour. Sci. Technol.*, vol. 19, no. 6, pp. 065015-1–065015-10, Nov. 2010.

[22] G. D. Stancu, F. Kaddouri, D. A. Lacoste, and C. O. Laux, "Atmospheric pressure plasma diagnostics by OES, CRDS and TALIF," *J. Phys. D, Appl. Phys.*, vol. 43, no. 12, pp. 124002-1–124002-10, Mar. 2010.
[23] *SIGLO Database*. [Online]. Available: http://www.lxcat.net, accessed Jul. 1, 2014.
[24] *Phelps Database*. [Online]. Available: http://www.lxcat.net, accessed Jul. 1, 2014.
[25] *IST-Lisbon Database*. [Online]. Available: http://www.lxcat.net, accessed Jul. 1, 2014.
[26] *Morgan Database*. [Online]. Available: http://www.lxcat.net, accessed Jul. 1, 2014.
[27] G. J. M. Hagelaar and L. C. Pitchford, "Solving the Boltzmann equation to obtain electron transport coefficients and rate coefficients for fluid models," *Plasma Sour. Sci. Technol.*, vol. 14, no. 4, pp. 722–733, Oct. 2005.

Moon Soo Bak received the B.S. degree in mechanical and aerospace engineering from Seoul National University, Seoul, Korea, in 2007, and the M.S. and Ph.D. degrees in mechanical engineering from Stanford University, Stanford, CA, USA, in 2010 and 2014, respectively.

He is currently a Visiting Professor with the School of Mechanical Engineering, Sungkyunkwan University, Suwon, Korea. His current research interests include combustion, fluid dynamics, atmospheric pressure plasmas, and plasma-assisted combustion.

Mark A. Cappelli received the B.A.Sc. degree in physics from McGill University, Montréal, QC, Canada, in 1980, and the M.A.Sc. and Ph.D. degrees in aerospace science and engineering from the University of Toronto, Toronto, ON, Canada, in 1983 and 1987, respectively.

He is currently a Professor with the Department of Mechanical Engineering, Stanford University, Stanford, CA, USA. His current research interests include plasmas and gas discharges, including plasma diagnostics, as they apply to aerodynamic and space propulsion, combustion, material processing, fusion, natural phenomenon, and medicine.